Vegetation History and Archaeobotany (2022) 31:247–260
https://doi.org/10.1007/s00334-021-00852-z

ORIGINAL ARTICLE

# Vegetation dynamics and their response to Holocene climate change derived from multi-proxy records from Wangdongyang peat bog in southeast China

Lin Zhao[1] · Chunmei Ma[1,2] · Zhenming Wen[3] · Wei Ye[3] · Guangchun Shang[1] · Lingyu Tang[4]

Received: 27 September 2020 / Accepted: 13 May 2021 / Published online: 27 July 2021


## Abstract

The East Asian summer monsoon (EASM) significantly influences the precipitation and vegetation dynamics in that region. Previous studies have assessed the spatial and temporal dynamics of the EASM, however vegetation responses to Holocene climate change and their driving mechanisms are yet to be understood. In this study, our multi-proxy records from southeast China are used to better understand Holocene climate change and its effects on vegetation. These records reveal a warm and wet climate from ca. 8.0 to 2.0 ka cal BP, followed by a cooler and drier climate since ca. 2.0 ka cal BP. The extent of evergreen broadleaved forest decreased significantly after 2.0 ka cal BP, which was in response to the cooler and drier climate in this period. During the Mid Holocene, solar radiation was probably the dominant factor controlling climate variability. A higher frequency of the El Niño event and increased $CO_2$ concentration in the atmosphere, along with a rapid southward movement of the inter tropical convergence zone (ITCZ), resulted in the weakening of the EASM since the Late Holocene. An even cooler and drier climate was identified for ca. 7.5–7.2 ka cal BP, and this abrupt cooling event occurred earlier in southeastern than in northern China. There was a reduction in forest cover in response to this rapid climate change. Decreased solar radiation and the influx of meltwater into the North Atlantic were the probable causes of this event.

**Keywords** Vegetation dynamics · Abrupt climate events · East Asian summer monsoon · Southeast China · Multi-proxy records

## Introduction

Understanding the variability of the East Asian summer monsoon (EASM) is vital for predicting global climate change because this fluctuation is a significant part of the global climate system (Wang 2006; IPCC 2014). The variability of the Holocene climate has attracted significant attention because its most recent phase resembles the modern climate. Oxygen isotope records from ice cores indicate a generally stable climate during the Holocene (Dansgaard et al. 1993); however, studies such as those from Greenland ice cores and the North Atlantic ice-raft detritus records have identified abrupt Holocene climate changes (O'Brien et al. 1995; Bond et al. 1997). Sudden Holocene climate events have been extensively studied because of their rapid changes, large fluctuations and long durations (Alley et al. 2003; Chen et al. 2015). These events include those dated to ca. 8.2 ka (Park et al. 2019; Waltgenbach et al. 2020), ca. 5.5 ka (Wu et al. 2018), ca. 4.2 ka (Park et al. 2019; Pleskot et al. 2020) and ca. 2.8 ka cal BP (Park et al. 2019). The dates of these changes to the EASM and the areas affected by them have been studied (for example, Wang et al. 2005; Chen et al. 2015; Porter et al. 2019); however, such events, particularly those occurring at ca. 7.5–7.0 ka cal BP and their effects on the vegetation are yet to be clearly understood. Therefore, reliable palaeoclimatic records are needed with clear proxy evidence of the monsoon and with a good chronology.

Communicated by Y. Zhao.

✉ Chunmei Ma
chunmeima@nju.edu.cn

[1] School of Geography and Ocean Science, Nanjing University, Nanjing 210023, Jiangsu, China

[2] Jiangsu Collaborative Innovation Center for Climate Change, Nanjing 210023, China

[3] School of Geography and Environmental Science, Zhejiang Normal University, Jinhua 321000, China

[4] Nanjing Institute of Geology and Palaeonotology, Chinese Academy of Sciences, Nanjing 210008, China

The subtropical regions of southern China have numerous areas of particular vegetation diversity (Huang et al. 2016), which are particularly suitable for Holocene vegetation studies (Yue et al. 2012; Ma et al. 2016; Zhao et al. 2016, 2017). Southeastern subtropical China is a critical area for studying the variability of the EASM during the late Quaternary period because it lies in the path of the summer monsoon circulation (Wang et al. 2005). Major peat-based Holocene palaeoclimate research up to now in Zhejiang province has mainly studied sediment particle (grain) size, organic matter content and magnetic susceptibility (Li et al. 2019). Few studies have analysed the intensity of the abrupt Holocene climate events in southeast China, their mechanisms and the resulting responses of the ecosystem to them.

Pollen analyses of peat sediment in southeast China can help reconstruct Holocene EASM variability and determine its impact on the vegetation. A previous pollen study in this region together with analyses of sediment particle sizes and geochemicals was done on cores from Wangdongyang (WDY) peat bog, Zhejiang province, but it was not well dated or of high resolution (Gu et al. 2016). Our age model, which is supported by 13 accelerator mass spectrometry (AMS) $^{14}$C dates, suggests that the combined records from this site cover the period from ca. 8.3/8.1 ka cal BP to the present day. The period ca. 7.5–7.2 ka cal BP shows significant reductions in the content of Si, Al, Ti and Fe, along with a reduction in the average sediment particle size and percentages of evergreen broadleaved trees, which suggest a cooler, drier climate. This study aims to explore Holocene climate change, particularly the abrupt climatic events that occurred at ca. 7.5–7.0 ka cal BP and the natural variability of the EASM. Our study provides new understanding of the vegetation dynamics and their response to Holocene climate change in the East Asian monsoon region.

## Materials and methods

### Regional setting

The Wangdongyang (WDY) peat bog (cores WDY1: 27° 40′ 48″ N, 119° 38′ 15″ E, 1,303 m a.s.l.; WDY2: 27° 40′ 58″ N, 119° 38′ 15″ E, 1,300 m) is located in the Shangbiao forest in Jingning county, which lies in the southern part of Zhejiang province in southeastern China (Fig. 1b, c). It is the most developed inland high altitude swamp in eastern China and the climate there is warm and moist, and it is controlled by the monsoon circulation (Domrös and Peng 1988). The mean annual temperature is 12 °C and the mean temperatures of January and July are 1.8 °C and 21.8 °C respectively (Wen et al. 2018). There is significant rainfall, with a mean annual precipitation of 2,067 mm (Wen et al. 2018) and the abundant rains occurring from June to September contribute to the moist regional climate. Most rainfall occurs in June in response to the start of the fully developed EASM. The regional geology shown by the main exposed strata in the region is of pre-Sinian metamorphic, Jurassic volcanic and Cretaceous sedimentary rocks, along with overlying loose Quaternary sediments (Gu et al. 2016). The study region lies within the subtropical climate zone (Domrös and Peng 1988) and has a diverse and rich forest vegetation (Gu et al. 2016). The majority of our study area is covered by forests, open grasslands and cultivated land. It can be described as a mountainous terrain, with a favourable climate and a relatively low population density. The vegetation in this region includes evergreen and deciduous broadleaved mixed forests with some conifers (Fig. 1c). The main trees found in these forests are *Pinus massoniana* Lambert, *Cunninghamia lanceolata* (Lamb.) Hook (Taxodiaceae-type) and the bamboo *Phyllostachys edulis* (Carrière) Houzeau. Evergreen broadleaved species include *Cyclobalanopsis glauca* (Thunb.) Oerst., *Castanopsis eyrei* (Champ.) Tutch., *C. sclerophylla* (Lindl.) Schott., *C. carlesii* (Hemsl.) Hay., and *Ilex chinensis* Sims. Deciduous broadleaved species are *Quercus fabri* Hance, *Q. acutissima* Carruth., *Q. variabilis* Bl., *Q. glandulifera* Bl., *Liquidambar formosana* Hance and others (Ministry of Forestry 1993; Lu and Ye 2014). The plant communities are rich and diverse, and the main trees grow in several different types of woodland; *Alnus trabeculosa* Hand.-Mazz. is one of the most abundant trees in the wetland of this region (Gu et al. 2016; Wen et al. 2018).

For our study, we analysed two cores, about 300 m apart, obtained from the centre of Wangdongyang which reached the bottom of the peat bog. We used a manual corer to do this sampling, obtaining two cores from several borings which were collected in PVC tubes 60 mm in diameter and 50 cm in length. Both sediment cores were sub-sampled in the laboratory at intervals of 1 cm, giving totals of 105 and 61 samples from WDY1 and WDY2, which were analysed for pollen at 2 cm intervals. Particle size analysis was done on 98 samples from WDY1, at 2 and 4 cm intervals and 184 samples at 1 cm intervals were analysed using X-ray fluorescence (XRF) for determining the elemental composition.

### Dating

Nine plant macrofossil and four peat samples from WDY1 and WDY2 were submitted to Beta Analytics (USA) for AMS $^{14}$C dating (Table 1). Some dates for WDY2 were also obtained from Wen et al. (2018). All $^{14}$C dates were converted to calendar years with the IntCal20 calibration curve (Reimer et al. 2020). Bayesian chronological modelling is the most frequently used way of studying the dates and it integrates the data into a coherent framework and gives estimates of age–depth relationships objectively and optimally (Bronk Ramsey 2009). This was done using BACON v. 2.5.0 (Blaauw and Christen 2011) for the chronology (Fig. 2), also using R v.3.3.2 (R Core Team 2020).

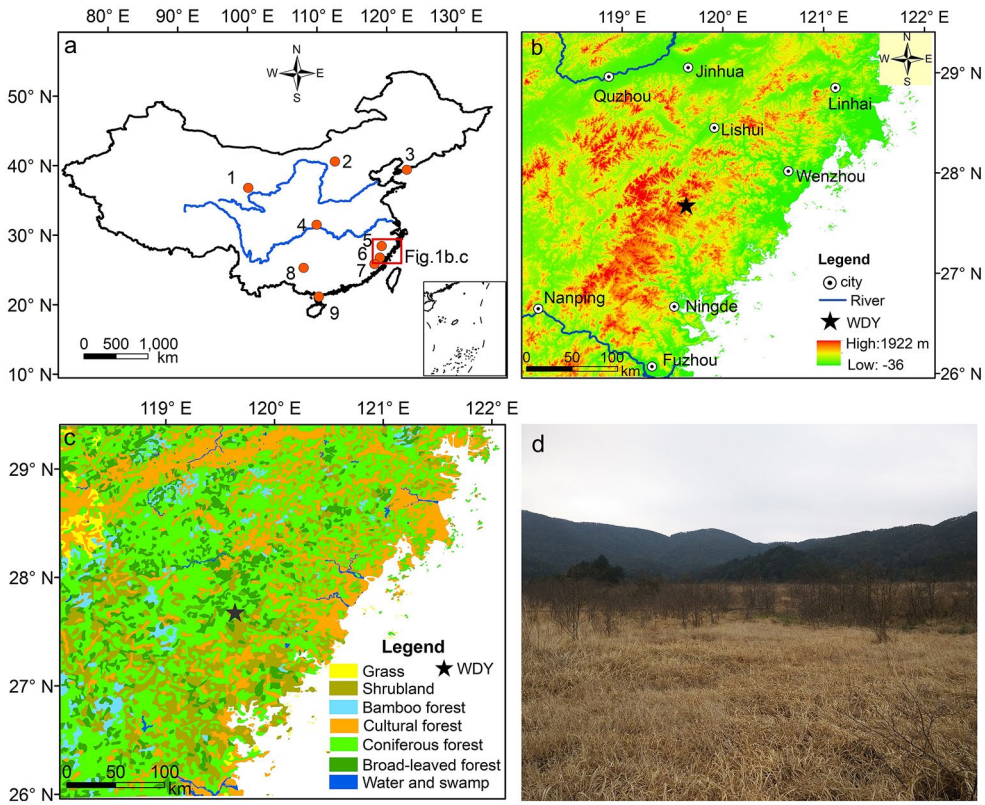


**Fig. 1** **a** Study locations, 1 Qinghai lake (An et al. 2012), 2 Daihai Lake (Xiao et al. 2004), 3 core from northern Yellow Sea (Nan et al. 2017), 4 Dajiuhu peat bog (Zhu et al. 2010), 5 Lantianyan peat bog (Ma et al. 2016), 6 Shuizhuyang (SZY) core in the Pingnan peat bog (Yue et al. 2012), 7 Daiyunshan peat bog (Zhao et al. 2017), 8 Dongge Cave (Wang et al. 2005), 9 Huguangyan maar (Wang et al. 2007). **b** Digital elevation map of the study area, **c** vegetation map (Editorial Committee of Vegetation Map of China 1980), and **d** photo of Wangdongyang (WDY) site

**Table 1** Details of the AMS dated samples and calibrated ages

| Lab. code | Sample no | Depth (cm) | $\delta^{13}C$ (‰) | Dating material | $^{14}C$ age (BP) | Cal age, 2σ-range (years cal BP) |
|---|---|---|---|---|---|---|
| Beta-494532 | WDY1-19-20 | 20–19 | NA | Plant macrofossil | 320 ± 30 | 463–306 |
| Beta-507565 | WDY1-40-41 | 41–40 | − 25.7 | Plant macrofossil | 210 ± 30 | 221–142 |
| Beta-507566 | WDY1-70-71 | 71–70 | − 28.5 | Plant macrofossil | 340 ± 30 | 475–312 |
| Beta-494531 | WDY1-99-100 | 100–99 | − 25.7 | Plant macrofossil | 400 ± 30 | 512–428 |
| Beta-507567 | WDY1-140-141 | 141–140 | − 28.0 | Plant macrofossil | 1,250 ± 30 | 1,276–1,196 |
| Beta-523689 | WDY1-161-162 | 162–161 | − 24.5 | Plant macrofossil | 4,690 ± 30 | 5,478–5,319 |
| Beta-494530 | WDY1-169-170 | 170–169 | − 25.5 | Plant macrofossil | 6,440 ± 30 | 7,425–7,307 |
| Beta-523690 | WDY1-185-186 | 186–185 | − 23.8 | Plant macrofossil | 6,500 ± 30 | 7,402–7,324 |
| Beta-507568 | WDY1-204-205 | 205–204 | − 26.4 | Plant macrofossil | 7,360 ± 30 | 8,211–8,032 |
| Beta-412736 | WDY2-19 | 20–18 | − 26.3 | Peat | 280 ± 30 | 455–355 |
| Beta-412737 | WDY2-69 | 70–68 | − 27.6 | Peat | 1,500 ± 30 | 1,413–1,307 |
| Beta-438866 | WDY2-99 | 100–98 | − 27.7 | Peat | 3,650 ± 30 | 4,019–3,885 |
| Beta-438867 | WDY2-121 | 122–120 | − 28.0 | Peat | 6,510 ± 30 | 7,399–7,326 |

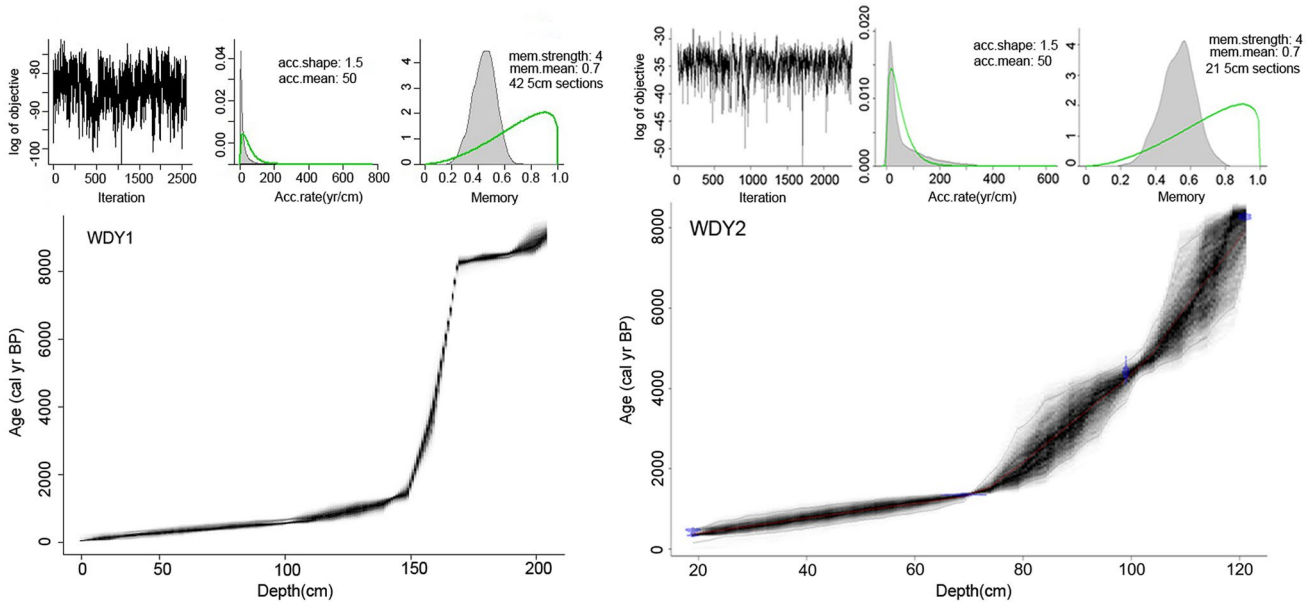


**Fig. 2** Age–depth model of cores WDY1 and 2. The 95% probability date ranges are within the grey area

## Proxy data analysis

The pollen and sediment particle size analyses were done at the School of Geography and Ocean Science at Nanjing University. Pollen was extracted according to the standard procedure (Fægri and Iversen 1989) and micro-charcoal particles were also studied in the pollen preparations. The sediment particle sizes were measured with a Malvern Mastersizer 2000 analyser, based on the method described by Lu and An (1998). We transformed the particle size distribution into various end-members in order to characterize the depositional environments more accurately (ESM 1; Weltje and Prins 2003). X-ray fluorescence (XRF) studies were done with an Avaatech core scanner at the XRF Laboratory at Nanjing University School of Earth Sciences and Engineering, with continuous high resolution (1 cm) micro-XRF element scanning. Principal component analysis (PCA) was done on the pollen percentages and geochemical elements with CANOCO v. 4.52 (Ter Braak and Smilauer 2003). Detailed descriptions of the procedures are in ESM 1, the data sets in ESM 2.

# Results

## Peat stratigraphy and age modelling

In WDY1, we identified seven distinct units of sediment, including yellowish-brown peat and brownish peat with silt (Fig. 3a); in WDY2, we identified six distinct units (Fig. 3b). No obvious sediment hiatuses or disturbances were noticed when we subsampled. The majority of the AMS dated samples in WDY1 and WDY2 were in chronological order in both cores, suggesting that the dating was good (Fig. 2; Table 1). Both records started in the Mid Holocene, with median bottom sample ages of ca. 8.3 and 8.1 ka cal BP. Sedimentation rates were moderately high in the bottom 40 cm of WDY1; the lowest sedimentation rates were at 169–140 cm, and the highest ones at 140 cm from the top of the peat section (Fig. 2). In WDY2, the lowest sedimentation rates were at 122–99 cm, moderately high at 99–69 cm and the highest rates at the top, at 69–18 cm (Fig. 2).

## Pollen results

We identified 99 pollen and spore types consisting of 55 trees and shrubs, 31 herbs, 6 wetland and aquatic taxa, 7 ferns and 6 types of algal palynomorphs. The main results are presented in simplified pollen diagrams in Fig. 3. The WDY1 pollen diagram (Fig. 3a) is divided into five major pollen assemblage zones whose key features are described below.

Zone 1 (210–169 cm; ca. 8.3–6.7 ka cal BP) is defined by high and stable arboreal pollen (AP) percentages (based on the total sum of terrestrial pollen, including trees, shrubs and terrestrial herbs), mainly evergreen *Quercus*, *Alnus* and Taxodiaceae, and relatively low percentages of dry land herbaceous pollen, wetland and aquatic herbs and fern spores throughout the zone. Poaceae and Cyperaceae are the main non arboreal pollen (NAP) types. The total pollen concentrations are relatively high at approximately 129,000 grains

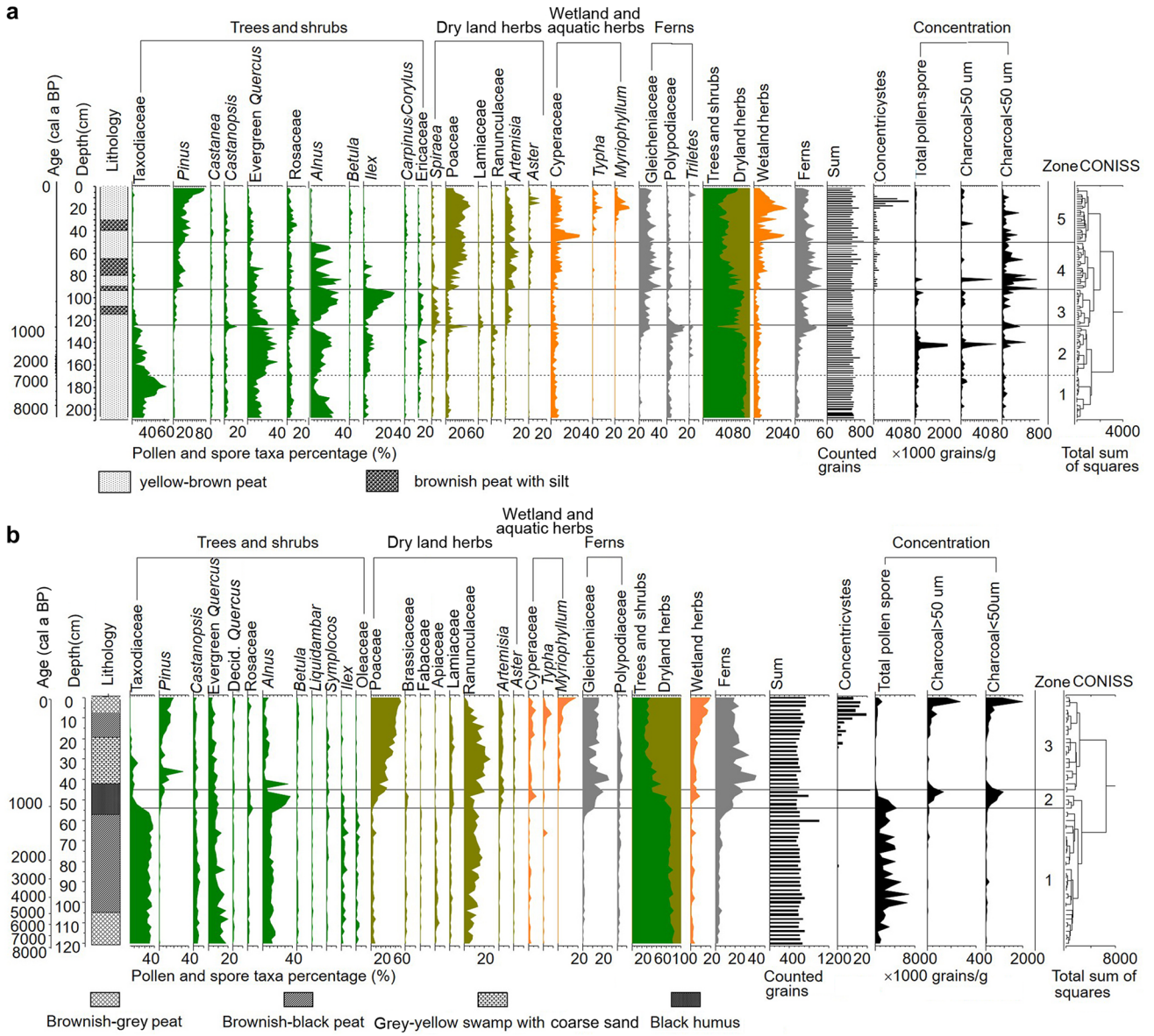


**Fig. 3** **a** WDY1 pollen diagram, and **b** WDY2 pollen diagram; pollen percentages of the total sum of terrestrial pollen, including trees, shrubs and terrestrial herbs. Percentages of wetland and aquatic herbs, ferns and algae are based on the total sum of all palynomorphs and algae

$g^{-1}$ but concentrations of charcoal are very low, mean 3,000 fragments $g^{-1}$.

Zone 2 (169–124 cm; ca. 6.7–0.9 ka cal BP) is dominated by evergreen *Quercus* which is also the most abundant taxon throughout the record. *Alnus*, *Ilex* and Taxodiaceae are the dominant pollen contributors in this zone. The AP percentages are high, but slightly lower than those in the other zones. The NAP percentages are low, and the values of fern spores relatively high. The pollen concentration is at its highest, with an average of 480,000 grains $g^{-1}$. There is a charcoal concentration peak of > 77,000 fragments $g^{-1}$ at approximately 141 cm from the surface.

Zone 3 (124–92 cm; ca. 0.9–0.5 ka cal BP) is characterized by a dominance of tree pollen (66–91%). The amount of Taxodiaceae pollen is negligible, but *Ilex* pollen is significantly higher at 15–40% of the total pollen assemblage. The values of evergreen *Quercus* are lower, but *Alnus* has a peak of approximately 30%. Percentages of dry land herbs and ferns are higher than in previous zones, while those of wetland and aquatics herbs are lower. The total pollen and charcoal concentrations are moderate to low, but are relatively higher in the upper part of this zone (ca. 0.5 ka cal BP).

Zone 4 (92–50 cm; ca. 0.5–0.25 ka cal BP) is distinctly different from the others because of its markedly lower AP percentages, in which evergreen *Quercus* and *Alnus* remain

dominant. Although the percentages of wetland and aquatic herbs remain low, those of dry land herbs and ferns are higher in the upper part above 75 cm (ca. 0.4 ka cal BP). The total pollen concentration is relatively low (approximately 70,000 grains $g^{-1}$), and there is a distinct charcoal concentration peak of > 68,000 fragments $g^{-1}$ at approximately 83 cm.

Zone 5 (50–0 cm; ca. 0.25–0 ka cal BP) is also characterized by a dominance of evergreen *Quercus* (4% mean), but other trees including *Castanea*, *Alnus* and *Ilex* are relatively scarce. The highest proportions of Poaceae and *Pinus* occur in this zone. Fern spores are relatively abundant, and the percentages of wetland and aquatics and dry land herbs are notably higher. The total pollen concentration is very low (approximately 57,000 grains $g^{-1}$), and there is a moderate charcoal concentration peak of 26,000 fragments $g^{-1}$ at about 33 cm.

The WDY2 pollen diagram is divided into three major zones which are described below (Fig. 3b).

Zone 1 (122–56 cm; ca. 8.1–1.0 ka cal BP) is characterized by stable and high AP percentages (79.5% mean), mainly evergreen *Quercus*, *Alnus* and Taxodiaceae and relatively small amounts of dry land herbs, wetland and aquatic herbs and fern spores. Ranunculaceae is a major NAP taxon found in this zone. The total pollen concentrations are high (approximately 129,000 grains $g^{-1}$) and the charcoal concentrations are very low.

Zone 2 (56–46 cm; ca. 1.0–0.9 ka cal BP) is dominated by *Alnus* pollen, as well as evergreen *Quercus*, *Ilex* and *Castanopsis*. The AP percentages are very high, but slightly lower than those in zone 1. The NAP percentages are low and the fern spores relatively high. Pollen concentrations are the highest in this zone (average of 1,910,000 grains $g^{-1}$). The > 50 µm and < 50 µm charcoal concentration peaks at an approximate depth of 48 cm are 133,000 fragments $g^{-1}$ and 937,000 fragments $g^{-1}$, respectively.

Zone 3 (46–0 cm; ca. 0.90 ka cal BP) has significantly lower percentages of AP, mainly *Ilex*, *Alnus* and *Castanopsis*. Taxodiaceae pollen is present in small amounts, but Poaceae is higher than in the other zones at 15–60% of the total pollen assemblage. Evergreen *Quercus* is lower, while dry land herbs, wetland and aquatic herbs and fern spores are higher; *Pinus* pollen peaks at approximately 32% in this zone. The total pollen and charcoal concentrations are moderate to low, but are relatively higher in the upper part (ca. 0.4 ka cal BP).

A detailed description of the principle components analysis (PCA) of the pollen results is given in ESM 1, Fig. S1.

## Particle size and geochemistry results

In our study area, the East Asian monsoon brings most of the precipitation, which has over the years accumulated water in the basin to form a peat bog. The particle size of the mineral input is influenced by its source and the relative changes in the water level. The changes in particle size mainly reflect the influence of either dry or wet climates. When the EASM is stronger and brings more precipitation, there is more erosion washing in fine silt material.

The particle size distribution from WDY1 is relatively uniform, with most samples having particle sizes of 4–64 µm and only a few were < 4, or larger at 70–120 µm. The median particle size fluctuates greatly in the 6–40 µm range, and a few samples showed peaks between 40 and 130 µm. End member modelling analysis was done to distinguish the different groups of particle sizes (ESM 1). $R^2$ indicates the linear correlations between end members and the original data set. The higher value of $R^2$, the better the fit and the representativeness between end members and the original data set. The mean total $R^2$ between the modelled and original data is generally > 0.9, based on this analysis. The end members EM1 to EM4 explain 68, 22.9, 4.5 and 1.6% of the data variance and show particle sizes that are in the ranges of 0.3–1000, 0.8–600, 10–2000 and 15–2000 µm, with peaks at ~ 1.4, ~ 11, ~ 40 and ~ 560 µm (Fig. 4). EM1 and EM2 consist of fine silt, EM3 coarse silt and EM4 coarse sand. Since there were more of them, we concentrated on the EM1 and EM2 components. These are most sensitive to climate change and they are relatively stable between ca. 8.3 and 1.5 ka cal BP, but show high variability after ca. 1.5 ka cal BP (Fig. 5h, i).

The geochemical analysis studied the main minerals in the sediment. Macroelements are the main chemical components of rocks and sediments, and their content changes are mainly those of the main minerals, which can show the source of the sediments. Al, Si, Ti, and Fe represent rock fragments brought in from elsewhere (Schreiber et al. 2014; Rothwell and Croudace 2015). These minerals are sensitive to climate change and have often been used to show the climatic environment of the source region (Cuven et al. 2010; Kylander et al. 2011). In our samples they were present in large amounts, indicating more material brought in from the soil by high precipitation.

The geochemical elements are relatively uniform in WDY1 with high Al, Si, Ti and Fe concentrations from ca. 8.3 to 1.0 ka cal BP, representing minerals transported from elsewhere (Figs. 4c, 5d–g). This indicates increased amounts of material derived from various rock fragments in slope surface runoff and the formation of marshlands under a moist climate. The Al, Si, Ti, and Fe concentrations decrease noticeably from ca. 1.0 to 0.25 ka cal BP and then increase after ca. 0.25 ka cal BP, indicating a transition from low to high input of this material, which is most likely to have been in response to a climate change from dry to wet conditions. A detailed description of the principle components analysis (PCA) results for geochemical

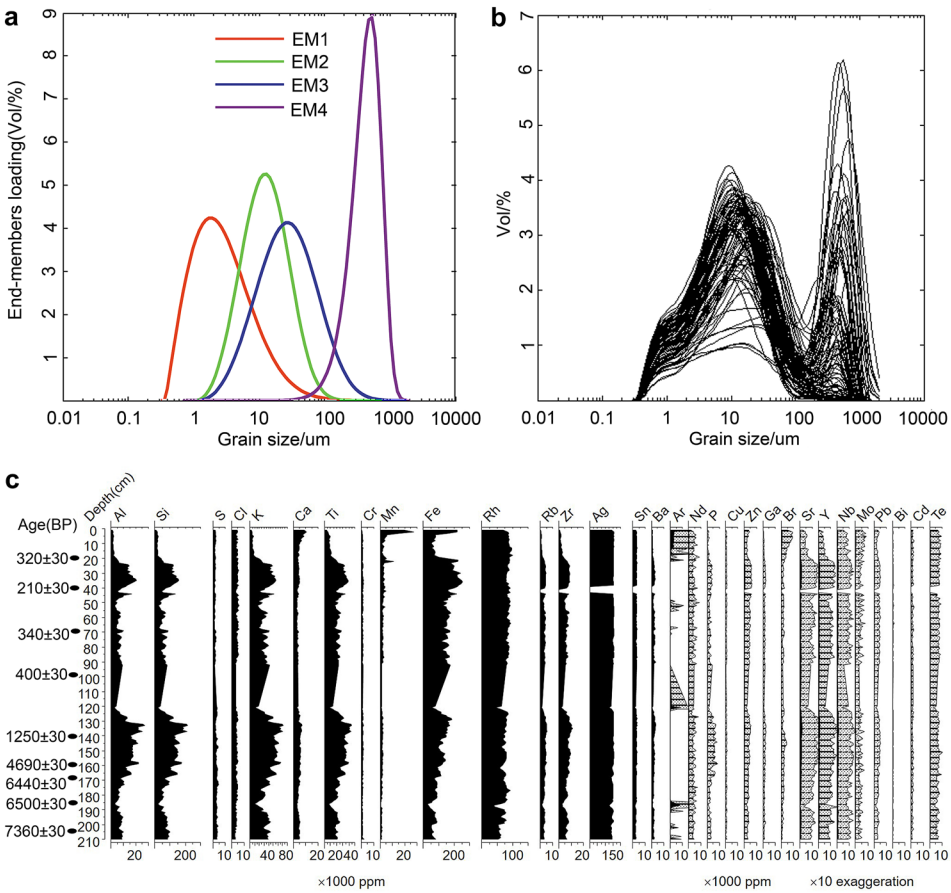


**Fig. 4** Sediment particle size distributions and geochemistry of WDY1; **a** results of optimal end-member modelling, **b** particle size distributions, and **c** geochemical element diagram

elements and their palaeoclimatic significance is provided in ESM 1, Fig. S2.

## Discussion

### Vegetation and other responses to changes in the East Asian summer monsoon

The Wangdongyang peat bog is in an enclosed basin without an outflow. The pollen sources are both local and regional so that the local pollen reflects the nearby surrounding vegetation and climate, which is important for understanding changes to the local vegetation (Prentice 1985; Xu and Zhang 2013). The regional pollen source is an area of 100–2,000 m from the centre of the basin and the pollen spectra also represent regional changes in the vegetation and thus the climate (Nielsen and Sugita 2005; Xu and Zhang 2013).

In this study, vegetation history of the Wangdongyang region during the Holocene has been reconstructed based on the pollen records. The high percentage of trees and the dominance of evergreen taxa during the Mid Holocene interval suggest a subtropical evergreen broadleaved forest vegetation (Fig. 5a, b). The high percentages of *Castanopsis* and evergreen *Quercus* and extremely low percentages of *Pinus* indicate a wet and warm climate, which favours evergreen broadleaved forests. The pollen records suggest a slight reduction in forest cover since ca. 2.0 ka cal BP, which is indicative of a relatively cool and dry climate. The concentration of charcoal increases and fluctuates then, which may indicate a phased drying of the climate. The high values in Axis 1 in the WDY1 and WDY2 PCAs also indicate a cool and dry climate (ESM 1, Fig. S1).

The high contents of Al, Si, Ti and Fe combined with the stable particle sizes for this part of the record (ca. 8.3/8.1–2.0 ka cal BP) suggest a warm and moist climate (Fig. 5d–g). The pollen, particle size and geochemical data indicate a stronger EASM during this period, which is supported by other pollen records from the lakes Gonghai (Chen et al. 2015), Daihai (Xiao et al. 2004) and Qinghai (Shen et al. 2005). These findings suggest that this region had a wetter climate and stronger summer monsoon during this part of the Holocene than today, which are also consistent with the pollen records from Fujian to the south of WDY (Zhao et al. 2016, 2017) and Taiwan to the southeast (Liew et al. 2006; Lee et al. 2010).

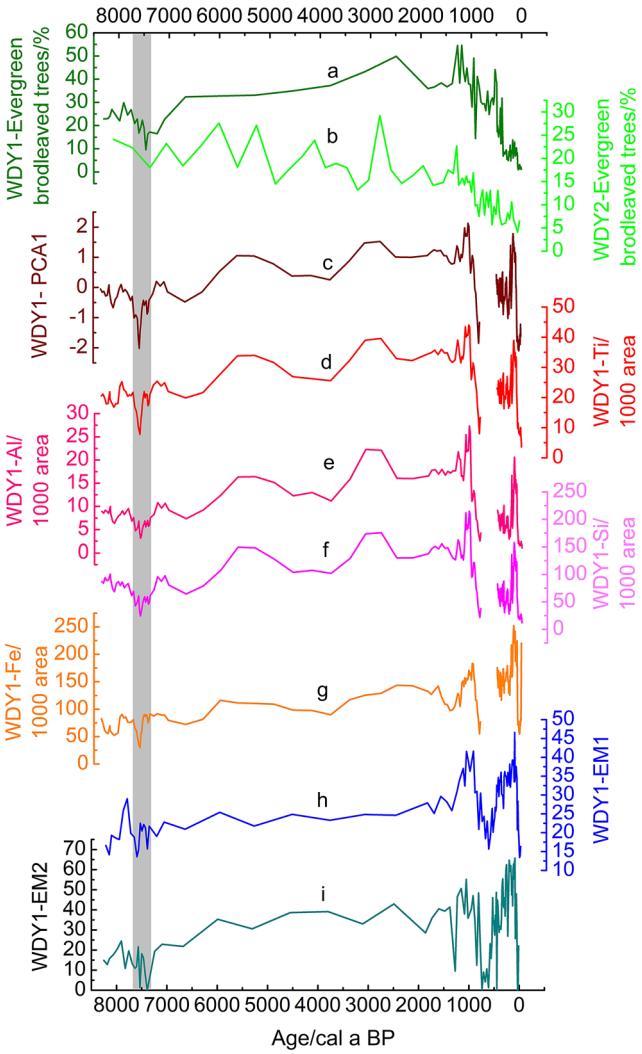


**Fig. 5** Summary plot of evergreen tree pollen percentages in (a) WDY1, (b) WDY2, (c) principal component analysis (PCA) axis 1 of geochemical elements in WDY1, elements in WDY1, (d) Ti, (e), Al, (f) Si, (g) Fe, (h, i) particle classes EM1 and EM2 in WDY1

In the period ca. 7.5–7.2 ka cal BP there were significant reductions of sediment particle sizes and concentrations of Si, Al, Ti and Fe, indicating a drier and cooler climate, consistent with the pollen records from the East Asian monsoon region of China (Zhu et al. 2010; Zhao et al. 2017). This period is also characterized by low values of evergreen taxa in response to the climate change.

In the period ca. 6.7–2.0 ka cal BP the large amounts of Al, Si, Ti, Fe and the fine EM1 and EM2 sediment components indicate a high and stable input of mineral materials (Fig. 5), suggesting a warm and moist climate. The obvious peaks in the pollen percentages of evergreen *Quercus*, *Ilex* and *Alnus* reflect the shorter term climate fluctuations over centuries superimposed on the more gradual longer term changes over millennia (Fig. 3). In WDY1, *Quercus* pollen percentages rapidly increase to a maximum of 29% during this period, which indicates a localized spread of oaks under wetter and warmer climate conditions.

In the Late Holocene (ca. 2.0 ka cal BP), the amounts of Al, Si, Ti and Fe and the finer particle size fractions EM1 and EM2 decrease and fluctuate strongly, indicating a low and unstable input of mineral materials under cool and dry climate conditions. The highest percentages of xerophytic taxa with *Aster*, *Artemisia*, *Taraxacum* and Chenopodiaceae occur in this part of WDY1 and WDY2 (Fig. 3) and they also indicate drier conditions, which is consistent with other precipitation reconstructions of the East Asian monsoon region (Chen et al. 2015; Lu et al. 2019; Sun et al. 2019). The WDY1 and WDY2 pollen records indicate a slight reduction in forest cover, which is supported by a slight increase in the percentages of herbs and fern spores. Additionally, the other Late Holocene records cited in this study suggest that these areas received less precipitation during this period than in the Mid Holocene and were covered by deciduous trees.

In the period ca. 2.0–0.9 ka cal BP the Al, Si, Ti and Fe concentrations, evergreen *Quercus* pollen percentages and the fine EM1 and EM2 particle sizes are relatively high, indicating a continuing relatively warm and wet climate. At ca. 0.9–0.2 ka the percentages of *Alnus* pollen in WDY1 and WDY2 increase significantly, accompanied by a marked reduction of evergreen *Quercus* pollen. This suggests a fairly warm and wet climate during the Medieval Warm Period (MWP), despite the relatively lower temperatures and precipitation than in the previous period. There is a pronounced reduction in Al, Si, Ti and Fe concentrations and in the EM1 and EM2 particle size components during the period ca. 0.5–0.25 ka cal BP, indicating drier and cooler conditions during the early Little Ice Age (LIA), compared to the MWP. During the LIA, the percentages of evergreen *Quercus*, *Ilex* and *Alnus* pollen decrease markedly, representing a reduction in the wooded areas and indicating drier and cooler climate conditions. Pollen evidence from the Daiyunshan mountain peat bog (Zhao et al. 2016, 2017) also suggests a reduction in the forest cover as the climate became cooler and drier from the MWP to the LIA. This climatic pattern has also been observed in regional and global records (Mann et al. 2008; Ge et al. 2013; PAGES 2k Consortium 2019). Interestingly, the Al, Si, Ti and Fe concentrations and EM1 and EM2 particle size classes increased after ca. 0.25 ka cal BP, coinciding with a reduction in the tree pollen percentages. This suggests that the climate was relatively dry and cold during the late LIA, resulting in strong climatic fluctuations and inconsistent inputs of mineral materials.

A strong reduction in AP percentages after 2 ka cal BP may reflect climate more than human impact. However, there is not enough direct evidence to suggest a large human population and significant regional scale impact on the vegetation and landscape of the study area before 2 ka cal BP. The

research focus of this paper is on climate change and vegetation change rather than on human activity. In a future paper we will combine the results from several peatland research sites in southeastern China to discuss human activities after 2 ka cal BP in detail.

## Changes in solar radiation

This study also investigated the factors, which may have caused the climate and vegetation changes since the Mid Holocene. During this period, stronger solar radiation in summer caused greater thermal gradients between land and sea, which increased the intensity of the monsoon circulation, thereby increasing the flow of water vapour to the middle and lower Yangtze River area, which increased summer precipitation there (Laskar et al. 2004). Moreover, solar radiation can influence the intensity of atmospheric circulation (Gray et al. 2010). The associated energy decreases the amount of radiation reaching the ocean surface, which reduces moisture evaporation and transport and affects the EASM directly (Meehl et al. 2009). Similarly, the weakening of the EASM from lower solar radiation during the Late Holocene has been well recorded (Fig. 6g; Wang et al. 2005). A TraCE transient simulation of the lower Yangtze River area suggested a decrease in the average regional summer precipitation from the Early to Late Holocene, in response to the changes in the summer insolation (Lu et al. 2019). The dominant cause of climate change during the Mid to Late Holocene, when compared with that of the modern climate, is probably linked to the orbital variability of incoming solar radiation (Fig. 6f; Berger 1978). The evidence of significant evergreen and deciduous forest decrease after 2.0 ka cal BP is a response to a cool and dry climate during this period resulting from the reduction in solar radiation. In summary, the results of this study suggest that vegetation and palaeoclimate variations in southeast China since the Mid Holocene have been driven by changes in insolation.

## The effects of ice in the northern hemisphere and $CO_2$

Ice volumes in high northern latitudes have a dominant effect on the variability of the EASM in glacial and interglacial timescales (Ding et al. 1995, 2002). The ice volume in the northern hemisphere was relatively high during the Early Holocene and subsequently decreased since the Mid to Late Holocene (Dyke 2004). This decrease in the ice volume increased the ocean to land moisture transport distance, causing decreased summer precipitation (Ding et al. 2005). During the Holocene, summer precipitation in southern China was mainly controlled by the EASM and movement of inter tropical convergence zone (ITCZ). When the ITCZ rapidly moved southwards, it caused the EASM to weaken

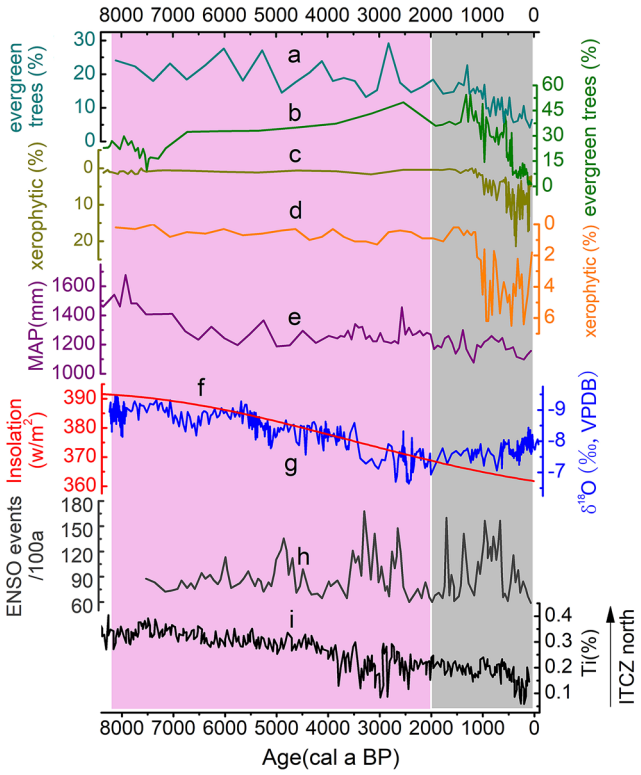


**Fig. 6** Comparison of WDY1 and 2 pollen and other records; (a) pollen percentages of evergreen trees in WDY1, (b) in WDY2, (c) pollen percentages of xerophytic taxa in WDY1, (d) in WDY2; other records, (e) mean annual precipitation reconstruction from Dajiuhu (Sun et al. 2019), (f) June to August insolation at 65° N (Berger 1978); (g) $\delta^{18}O$ record of Dongge Cave (Wang et al. 2005), (h) ENSO (El Niño Southern Oscillation) events per 100 years (Moy et al. 2002), (i) Ti concentration record from Cariaco Basin, which indicates movement of the ITCZ (inter tropical convergence zone) (Haug et al. 2001)

since the Late Holocene (Fig. 6i; Haug et al. 2001) and the summer precipitation decreased in southern China. Alternatively, higher atmospheric $CO_2$ concentrations may have raised the ocean surface temperatures and influenced the summer monsoon rainfall (Hu et al. 2000). The increasing effect of the El Niño-Southern Oscillation (ENSO, Fig. 6h; Moy et al. 2002) during the Holocene was accompanied by a gradual increase of the $CO_2$ concentration, indicating a possible relationship between $CO_2$ levels and precipitation. In contrast to the gradual decrease in insolation during the Late Holocene, the EASM declined abruptly at ca. 3.0 ka cal BP, which is attributed to tropical ocean conditions. During El Niño events, the tropical eastern Pacific Ocean warming increases the temperatures in the troposphere and causes an eastward propagation of the Kelvin wave, which increases the tropospheric temperature of the western Pacific Ocean (Chiang and Sobel 2002; Xie et al. 2009) and reduces the land to sea temperature difference and the effects of the EASM (Chen et al. 2015). These simulation results suggest

a higher frequency of the El Niño event during the Late Holocene, resulting in the weakening of the EASM. Therefore, solar radiation has probably been the dominant factor controlling climate changes during the Early to Mid Holocene. We can deduce that the higher frequency of the El Niño event and increased $CO_2$ concentration, together with a rapid southward movement of the ITCZ during the Late Holocene, have contributed to the weakening of the EASM. These changes to the EASM and other climatic factors led to a reduction in the evergreen broadleaved forest cover since the Mid Holocene.

## Abrupt climatic event at ca. 7.5–7.2 ka cal BP

The most notable changes which have been noticed for the period ca. 7.5–7.2 ka cal BP are the decreased Al, Si, Ti and Fe concentrations, the reductions in the EM1 and EM2 fine mineral particle classes and the reduced evergreen broadleaved tree cover, which together imply a drier and cooler climate (Fig. 5). This is confirmed by peat bog pollen records from Dajiuhu (Fig. 7e; Zhu et al. 2010), Lantianyan (Fig. 7f; Ma et al. 2016), Pingnan (Fig. 7g; Yue et al. 2012) and Daiyunshan (Fig. 7i; Zhao et al. 2017) and the Hugangyan Crater Lake (Fig. 7j; Wang et al. 2007) in southeast China, which also show a significant decrease in evergreen and other trees in this period, coinciding with a weakened EASM, as interpreted from the oxygen isotope ratio ($\delta^{18}O$) from a stalagmite obtained from the Dongge cave speleothem (Fig. 7d; Wang et al. 2005). The precipitation reconstructions from the Dajihu peat bog (Sun et al. 2019) and Xinjie regions (Lu et al. 2019) in the lower reaches of the Yangtze River in the East Asian monsoon region, indicate low precipitation from ca. 7.5–7.2 ka cal BP and both these studies show lower precipitation and temperatures in southeast China during this period, in response to a weaker EASM. Moreover, the low tree pollen percentages (Fig. 7a; Xiao et al. 2004) and decreased ocean surface temperature (Fig. 7b; Nan et al. 2017) in northern China at ca. 7.2–7.0 ka cal BP also occurred in response to the weakening of the EASM, as inferred from the Asian summer monsoon index obtained for Qinghai lake (Fig. 7c; An et al. 2012) and the $\delta^{18}O$ speleothem records obtained from the Nuanhe (Wu et al. 2011) and Wangjiawei Caves (Dong and Zhang 2012), suggesting that this abrupt climate event occurred later in northern than in southeastern China.

The ca. 7.5–7.0 ka cal BP event has featured in palaeoclimatic records worldwide. For example, the argon and nitrogen isotope records from the Greenland ice core GISP2 suggest a significant temperature decrease from ca. 7.5 to 7.0 ka cal BP (Kobashi et al. 2017) and North Atlantic deep sea sediments suggest a peak of ice-rafted debris at ca. 7.5–7.2 ka cal BP, indicating a significant cooling period (Bond et al. 2001). Temperature decreases in North America

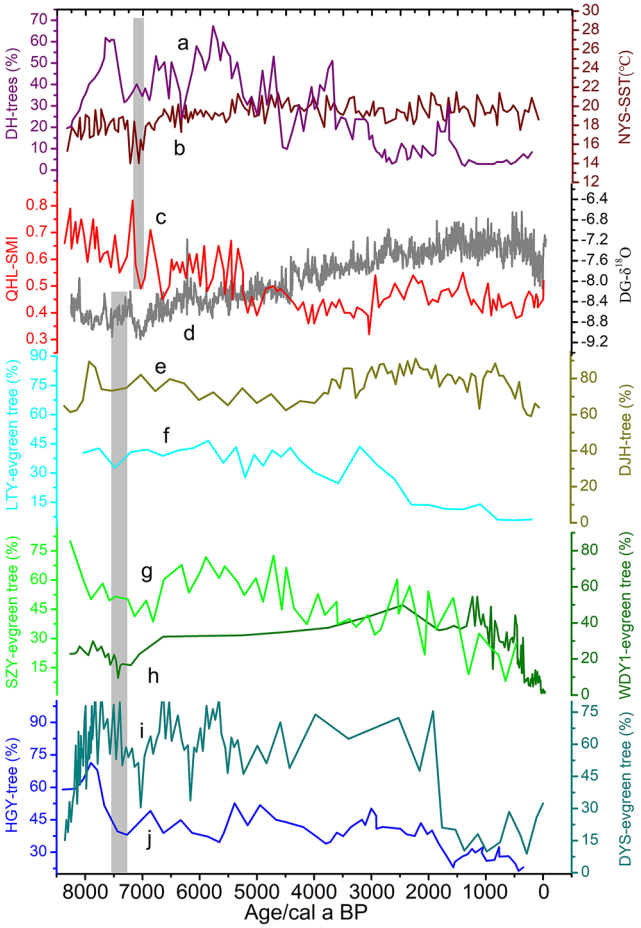


**Fig. 7** Selected palaeoclimate results demonstrating the cooling events since the Mid Holocene; (a) pollen percentages from Daihai Lake (Xiao et al. 2004), (b) sea surface temperature (SST) change in Huanghai Sea (Nan et al. 2017), (c) Asian summer monsoon index at Qinghai Lake (An et al. 2012), (d) $\delta^{18}O$ speleothem record from Dongge Cave (Wang et al. 2005), (e) pollen percentages from Dajiuhu (Zhu et al. 2010), (f–i) pollen percentages of evergreen broadleaved trees, (f) from Lantianyan (Ma et al. 2016), (g) Shuizhuyang (SZY) core in Pingnan peat (Yue et al. 2012), (h) WDY1 (current study), (i) Daiyunshan (Zhao et al. 2017), (j) tree pollen percentages from Hugangyan Crater Lake (Wang et al. 2007)

(Hughes et al. 2006; Ersek et al. 2012) and Europe (Korhola et al. 2000) have also been identified during this period, which agree with the reconstruction of the temperature of Greenland (Cuffey and Cow 1997; Jansson and Kleman 2004). Various records have also identified reduced precipitation in the southeast Arabian peninsula (Neff et al. 2001; Fleitmann et al. 2003), the Mediterranean coast (Frisia et al. 2006) and Africa (Thompson et al. 2002; Zielhofer et al. 2017) since ca. 7.5–7.2 ka cal BP. On the whole, these results suggest that the ca. 7.5–7.0 ka cal BP event was a global phenomenon involving decreasing temperature and precipitation.

Previous research has identified a close relationship between the variations in the EASM intensity and solar

radiation (Gupta et al. 2005; Wang et al. 2005). Moreover, some studies have identified the influence of insolation on the extent and strength of the Walker circulation, which was found to further amplify climate change. Solar forcing peaks (the difference between the energy absorbed by the Earth and that radiated back into space) increase the energy input into the surface of the ocean, which increases evaporation and moisture transport to convergence zones by the trade winds (Meehl et al. 2009; Gray et al. 2010). This leads to greater precipitation, strengthening the Hadley and Walker circulations in the troposphere (Meehl et al. 2009). Solar forcing peaks also increase ultraviolet radiation, which stimulates additional stratospheric ozone production and ultraviolet absorption. This results in the differential warming of the stratosphere according to latitude, so that the tropical tropospheric circulation is modified and precipitation increased towards the poles (Meehl et al. 2009). Measurements of the cosmogenic radionuclide $^{10}$Be in the GISP2 ice cores revealed a significant reduction in total solar radiation (Steinhilber et al. 2009) and Laskar et al. (2004) noted a reduction in solar activity at ca. 7.5–7.0 ka cal BP. These findings suggest that changes in solar radiation were the dominant cause of the abrupt climatic events during this period. This cooling event coincided with North Atlantic ice-rafting events (Bond et al. 2001), suggesting that insolation influences hemispheric and global centennial changes through its impact on meridional circulation (in a north–south direction). Additionally, some studies have identified a significant rise in sea level in the period ca. 7.5–7.2 ka cal BP (Yu et al. 2007; Zong et al. 2007; Zhao et al. 2021), which is consistent with the observed fresh water inflow to the sea due to melting ice. This large influx of fresh water would have altered the sea surface temperature and salinity, which probably slowed the North Atlantic Meridional Overturning Circulation (AMOC; Törnqvist and Hijma 2012; Bakker et al. 2017), resulting in reduced atmospheric temperatures in the high northern latitudes. Additionally, heat would have been transported northwards by the Hadley cell of global tropical circulation, which probably caused a southward movement of the ITCZ that weakened the EASM (Haug et al. 2001; Schneider et al. 2014). These results suggest that solar radiation and North Atlantic fresh water inflow were the main causes for the cooling event that occurred around ca. 7.5–7.2 ka cal BP.

## Conclusions

The high resolution multi-proxy records from the two WDY peat cores analysed in our study suggest a wet and warm climate and a stronger EASM than at present from ca. 8.3 to 2.0 ka cal BP, followed by a cooler and drier period and a weakened EASM from ca. 2.0 to 0 ka cal BP. Thus, we can conclude that precipitation changes in southeast China since the Mid Holocene have occurred in response to variations in the EASM. Insolation has also probably been a dominant factor controlling climate change during the Mid Holocene. Other factors such as more frequent El Niño events, a greater $CO_2$ concentration and the rapid southward movement of the ITCZ during the Late Holocene may also have resulted in the weakening of the EASM. This study identified an abrupt cooling event at ca. 7.5–7.2 ka cal BP, which occurred earlier in southeastern than in northern China. A reduction in the forest cover occurred in response to this event, and its primary causes may have been influx of fresh meltwater into the North Atlantic and changes in solar activity.

**Supplementary Information** The online version contains supplementary material available at https://doi.org/10.1007/s00334-021-00852-z.

**Acknowledgements** This research was supported by the National Natural Science Foundation of China (Grant 41977389), the National Key R&D Program of China (Grants 2020YFC1521605 and 2016YFA0600501) and the National Natural Science Foundation of China (Grant 41807432).

## References

Alley RB, Marotzke J, Nordhaus WD et al (2003) Abrupt climate change. Science 299:2,005–2,010. https://doi.org/10.1126/science.1081056

An ZS, Colman SM, Zhou WJ et al (2012) Interplay between the Westerlies and Asian monsoon recorded in Lake Qinghai sediments since 32 ka. Sci Rep 2:619. https://doi.org/10.1038/srep00619

Bakker P, Clark PU, Golledge NR, Schmittner A, Weber ME (2017) Centennial-scale Holocene climate variations amplified by Antarctic Ice Sheet discharge. Nature 541(7635):72–76. https://doi.org/10.1038/nature20582

Berger AL (1978) Long-term variations of caloric insolation resulting from the Earth's orbital elements. Quat Res 9:139–167

Blaauw M, Christen JA (2011) Flexible palaeoclimate age–depth models using an autoregressive gamma process. Bayesian Anal 6:457–474. https://doi.org/10.1214/ba/1339616472

Bond G, Kromer B, Beer J et al (2001) Persistent solar influence on North Atlantic climate during the Holocene. Science 294:2,130–2,136. https://doi.org/10.1126/science.1065680

Bond G, Showers W, Cheseby M et al (1997) A pervasive millennial-scale cycle in North Atlantic Holocene and Glacial climates. Science 278:1,257–1,266. https://doi.org/10.1126/science.278.5341.1257

Bronk Ramsey C (2009) Bayesian analysis of radiocarbon dates. Radiocarbon 51:337–360. https://doi.org/10.1017/s0033822200033865

Chen FH, Xu QH, Chen JH et al (2015) East Asian summer monsoon precipitation variability since the last deglaciation. Sci Rep 5:11,186. https://doi.org/10.1038/srep11186

Chiang JCH, Sobel AH (2002) Tropical tropospheric temperature variations caused by ENSO and their influence on the remote tropical

climate. J Clim 15:2,616–2,631. https://doi.org/10.1175/1520-0442(2002)0152.0.CO;2
Cuffey KM, Cow GD (1997) Temperature, accumulation, and ice sheet elevation in central Greenland through the last deglacial transition. J Geophys Res Oceans 102:26,383–26,396. https://doi.org/10.1029/96jc03981
Cuven S, Francus P, Lamoureux SF (2010) Estimation of grain size variability with micro X-ray fluorescence in laminated lacustrine sediments, Cape Bounty, Canadian High Arctic. J Paleolimnol 44:803–817. https://doi.org/10.1007/s10933-010-9453-1
Dansgaard W, Johnsen SJ, Clausen HB et al (1993) Evidence for general instability of past climate from a 250-kyr ice-core record. Nature 364:218–220. https://doi.org/10.1038/364218a0
Ding ZL, Derbyshire E, Yang SL, Yu ZW, Xiong SF, Liu TS (2002) Stacked 2.6-Ma grain size record from the Chinese loess based on five sections and correlation with the deep-sea $\delta^{18}O$ record. Paleoceanogr Paleoclimatol 17:5-1-5–21. https://doi.org/10.1029/2001PA000725
Ding ZL, Derbyshire E, Yang SL, Sun JM, Liu TS (2005) Stepwise expansion of desert environment across northern China in the past 3.5 Ma and implications for monsoon evolution. Earth Planet Sci Lett 237:45–55. https://doi.org/10.1016/j.epsl.2005.06.036
Ding Z, Liu T, Rutter NW, Yu Z, Guo Z, Zhu R (1995) Ice-volume forcing of East Asian winter monsoon variations in the past 800,000 years. Quat Res 44:149–159. https://doi.org/10.1006/qres.1995.1059
Domrös M, Peng G (1988) The climate of China. Springer, Berlin
Dong JG, Zhang F (2012) The Mid Holocene climate variation inferred from a dated stalagmite record from Wangjiawei Cave, northeast China. Mar Geol Quat Geol 32:119–125. https://doi.org/10.3724/SP.J.1140.2012.01119
Dyke AS (2004) An outline of North American deglaciation with emphasis on central and northern Canada. Dev Quat Sci 2:373–424. https://doi.org/10.1016/S1571-0866(04)80209-4
Editorial Committee of Vegetation Map of China (Wu ZY) (1980) Vegetation map of China. Science Press, Beijing (**in Chinese**)
Ersek V, Clark PU, Mix AC, Cheng H, Edwards RL (2012) Holocene winter climate variability in mid-latitude western North America. Nat Commun 3:1,219. https://doi.org/10.1038/ncomms2222
Fægri K, Iversen J (1989). In: Fægri K, Kaland PE, Krzywinski K (eds) Textbook of pollen analysis, 4th edn. Wiley, Chichester
Fleitmann D, Burns SJ, Mudelsee M, Neff U, Kramers J, Mangini A, Matter A (2003) Holocene forcing of the Indian monsoon recorded in a stalagmite from southern Oman. Science 300:1,737–1,739. https://doi.org/10.1126/science.1083130
Frisia S, Borsato A, Mangini A, Spötl C, Madonia G, Sauro U (2006) Holocene climate variability in Sicily from a discontinuous stalagmite record and the Mesolithic to Neolithic transition. Quat Res 66:388–400. https://doi.org/10.1016/j.yqres.2006.05.003
Ge Q, Hao Z, Zheng J, Shao X (2013) Temperature changes over the past 2000 yr in China and comparison with the Northern Hemisphere. Clim Past 9:1,153–1,160. https://doi.org/10.5194/cp-9-1153-2013
Gray LJ, Beer J, Geller M et al (2010) Solar influences on climate. Rev Geophys 48:1,032–1,047. https://doi.org/10.1029/2009RG000282
Gu YS, Tang QQ, Liu HY, Qin YM, Tang XM (2016) Formation environment of the subalpine wetlands in Jingning She Autonomous County, Zhejiang Province. Wetl Sci 14:302–310. https://doi.org/10.13248/j.cnki.wetlandsci.2016.03.003 (**in Chinese with English abstracts**)
Gupta AK, Das M, Anderson DM (2005) Solar influence on the Indian summer monsoon during the Holocene. Geophys Res Lett 32:L17,703. https://doi.org/10.1029/2005gl022685
Haug GH, Hughen KA, Sigman DM, Peterson LC, Röhl U (2001) Southward migration of the intertropical convergence zone through the Holocene. Science 293:1,304–1,308. https://doi.org/10.1126/science.1059725
Hu ZZ, Latif M, Roeckner E, Bengtsson L (2000) Intensified Asian Summer Monsoon and its variability in a coupled model forced by increasing greenhouse gas concentrations. Geophys Res Lett 27:2,681–2,684. https://doi.org/10.1029/2000GL011550
Huang J, Huang J, Liue C, Zhang J, Lu X, Ma K (2016) Diversity hotspots and conservation gaps for the Chinese endemic seed flora. Biol Conserv 198:104–112. https://doi.org/10.1016/j.biocon.2016.04.007
Hughes PDM, Blundell A, Charman DJ, Bartlett S, Daniell JRG, Wojatschke A, Chambers FM (2006) An 8500 cal. year multiproxy climate record from a bog in eastern Newfoundland: contributions of meltwater discharge and solar forcing. Quat Sci Rev 25:1,208–1,227. https://doi.org/10.1016/j.quascirev.2005.11.001
IPCC (2014) In: Core Writing Team, Pachauri RK, Meyer LA (eds) Climate change 2014: synthesis report. Contribution of Working Groups I, II and III to the Fifth Assessment Report of the Intergovernmental Panel on Climate Change. IPCC, Geneva
Jansson KN, Kleman J (2004) Early Holocene glacial lake meltwater injections into the Labrador Sea and Ungava Bay. Paleoceanogr Paleoclimatol 19:PA1,001. https://doi.org/10.1029/2003PA000943
Kobashi T, Menviel L, Jeltsch-Thömmes A et al (2017) Volcanic influence on centennial to millennial Holocene Greenland temperature change. Sci Rep 7:1,441. https://doi.org/10.1038/s41598-017-01451-7
Korhola A, Weckström J, Holmström L, Erästö P (2000) A quantitative Holocene climatic record from diatoms in northern Fennoscandia. Quat Res 54:284–294. https://doi.org/10.1006/qres.2000.2153
Kylander ME, Ampel L, Wohlfarth B, Veres D (2011) High-resolution X-ray fluorescence core scanning analysis of Les Echets (France) sedimentary sequence: new insights from chemical proxies. J Quat Sci 26:109–117
Laskar J, Robutel P, Joutel F, Gastineau M, Correia ACM, Levrard B (2004) A long-term numerical solution for the insolation quantities of the Earth. Astron Astrophys 428:261–285. https://doi.org/10.1051/0004-6361:20041335
Lee CY, Liew PM, Lee TQ (2010) Pollen records in southern Taiwan, implications for East Asian summer monsoon variation during the Holocene. Holocene 20:81–89. https://doi.org/10.1177/0959683609348859
Li K, Jin YL, Tan B, Xu HF (2019) Development and climatic background of Dayanghu marsh peat from Jingning County, Zhejiang Province. Quat Sci 39:1,384–1,392. https://doi.org/10.11928/j.issn.10017410.2016.06.06 (**in Chinese with English abstracts**)
Liew PM, Lee CY, Kuo CM (2006) Holocene thermal optimal and climate variability of East Asian monsoon inferred from forest construction of a subalpine pollen sequence, Taiwan. Earth Planet Sci Lett 250:596–605. https://doi.org/10.1016/j.epsl.2006.08.002
Lu FZ, Ma CM, Zhu C et al (2019) Variability of East Asian summer monsoon precipitation during the Holocene and possible forcing mechanisms. Clim Dyn 52:969–989. https://doi.org/10.1007/s00382-018-4175-6
Lu HY, An ZS (1998) Paleoclimatic significance of grain size of loess-palaeosol deposit in Chinese Loess Plateau. Sci China D 41:626–631 (**in Chinese with English abstracts**)
Lu WC, Ye W (2014) Characteristics of pollen assemblage and climate change in the Holocene at Borehole BHQ in Pingyao area, Zhejiang Province. J Palaeogeogr 16:687–701. https://doi.org/10.7605/gdlxb.2014.05.55(inChinesewithEnglishabstracts)
Ma T, Tarasov PE, Zheng Z, Han AY, Huang KY (2016) Pollen- and charcoal-based evidence for climatic and human impact on vegetation in the northern edge of Wuyi Mountains, China, during the last 8200 years. Holocene 26:1,616–1,626. https://doi.org/10.1177/0959683616641744

Mann ME, Zhang ZH, Hughes MK, Bradley RS, Miller SK, Rutherford S, Ni FB (2008) Proxy-based reconstructions of hemispheric and global surface temperature variations over the past two millennia. Proc Natl Acad Sci USA 105:13,252–13,257. https://doi.org/10.1073/pnas.0805721105

Meehl GA, Arblaster JM, Matthes K, Sassi F, van Loon H (2009) Amplifying the Pacific climate system response to a small 11-year solar cycle forcing. Science 325:1,114–1,118. https://doi.org/10.1126/science.1172872

Ministry of Forestry (1993) Zhejiang forest. China Forestry Press, Beijing (**in Chinese**)

Moy CM, Seltzer GO, Rodbell DT, Anderson DM (2002) Variability of El Niño/Southern Oscillation activity at millennial timescales during the Holocene epoch. Nature 420:162–165. https://doi.org/10.1038/nature01194

Nan QY, Li TG, Chen JX, Chang FM, Yu XK, Xu ZK, Pi Z (2017) Holocene paleoenvironment changes in the northern Yellow Sea: evidence from alkenone derived sea surface temperature. Palaeogeogr Palaeoclimatol Palaeoecol 483:83–93. https://doi.org/10.1016/j.palaeo.2017.01.031

Nielsen AB, Sugita S (2005) Estimating relevant source area of pollen for small Danish lakes around AD 1800. Holocene 15:1,006–1,020. https://doi.org/10.1191/0959683605hl874ra

Neff U, Burns SJ, Mangini A, Mudelsee M, Fleitmann D, Matter A (2001) Strong coherence between solar variability and monsoon in Oman between 9 and 6 kyr ago. Nature 411:290–293. https://doi.org/10.1038/35077048

O'Brien SR, Mayewski PA, Meeker LD, Meese DA, Twickler MS, Whitlow SI (1995) Complexity of Holocene climate as reconstructed from a Greenland ice core. Science 270:1,962–1,964

PAGES 2k Consortium (2019) Consistent multidecadal variability in global temperature reconstructions and simulations over the Common Era. Nat Geosci 12:643–649. https://doi.org/10.1038/s41561-019-0400-0

Park J, Park J, Yi S, Kim JC, Lee E, Choi J (2019) Abrupt Holocene climate shifts in coastal East Asia, including the 8.2 ka, 4.2 ka, and 2.8 ka bp events, and societal responses on the Korean Peninsula. Sci Rep 9:10,806. https://doi.org/10.1038/s41598-019-47264-8

Pleskot K, Apolinarska K, Kołaczek P et al (2020) Searching for the 4.2 ka climate event at lake spore, Poland. CATENA 191:104,565. https://doi.org/10.1016/j.catena.2020.104565

Porter TJ, Schoenemann SW, Davies LJ, Steig EJ, Bandara S, Froese DG (2019) Recent summer warming in northwestern Canada exceeds the Holocene thermal maximum. Nat Commun 10:1,631. https://doi.org/10.1038/s41467-019-09622-y

Prentice IC (1985) Pollen representation, source area, and basin size: toward a unified theory of pollen analysis. Quat Res 23:76–86. https://doi.org/10.1016/0033-5894(85)90073-0

R Core Team (2020) R: a language and environment for statistical computing. R Foundation for Statistical Computing, Vienna. https://www.R-project.org/

Reimer PJ, Austin WEN, Bard E et al (2020) The IntCal20 northern hemisphere radiocarbon age calibration curve (0–55 cal kBP). Radiocarbon 62:725–757. https://doi.org/10.1017/RDC.2020.41

Rothwell RG, Croudace IW (2015) Twenty years of XRF core scanning marine sediments: what do geochemical proxies tell us? In: Groudace IW, Rothwell RG (eds) Micro-XRF studies of sediment cores. Springer, Dordrecht, pp 25–102

Schneider T, Bischoff T, Haug GH (2014) Migrations and dynamics of the intertropical convergence zone. Nature 513:45–53. https://doi.org/10.1038/nature13636

Schreiber N, Garica E, Kroon A, Ilsøe PC, Kjær KH, Andersen TJ (2014) Pattern recognition on X-ray fluorescence records from Copenhagen lake sediments using principal component analysis. Water Air Soil Pollut 225:2,221. https://doi.org/10.1007/s11270-014-2221-5

Shen J, Liu XQ, Wang SM, Ryo M (2005) Palaeoclimatic changes in the Qinghai Lake area during the last 18,000 years. Quat Int 136:131–140. https://doi.org/10.1016/j.quaint.2004.11.014

Steinhilber F, Beer J, Fröhlich C (2009) Total solar irradiance during the Holocene. Geophys Res Lett 36:L19,704. https://doi.org/10.1029/2009GL040142

Sun J, Ma CM, Cao XY, Zhao YT, Deng YK, Zhao L, Zhu C (2019) Quantitative precipitation reconstruction in the east-central monsoonal China since the Late Glacial period. Quat Int 521:175–184. https://doi.org/10.1016/j.quaint.2019.05.033

Ter Braak CJF, Smilauer P (2003) Canoco for Windows v. 4.52. Biometris, Wageningen

Thompson LG, Mosley-Thompson E, Davis ME et al (2002) Kilimanjaro ice core records: evidence of Holocene climate change in tropical Africa. Science 298:589–593. https://doi.org/10.1126/science.1073198

Törnqvist TE, Hijma MP (2012) Links between Early Holocene ice-sheet decay, sea-level rise and abrupt climate change. Nat Geosci 5:601–606. https://doi.org/10.1038/ngeo1536

Waltgenbach S, Scholz D, Spötl C et al (2020) Climate and structure of the 8.2 ka event reconstructed from three speleothems from Germany. Glob Planet Change 193:103,266. https://doi.org/10.1016/j.gloplacha.2020.103266

Wang B (2006) The Asian monsoon. Springer, Berlin

Wang SY, Lü HY, Liu JQ, Negendank JFW (2007) The Early Holocene optimum inferred from a high-resolution pollen record of Huguangyan Maar Lake in southern China. Chin Sci Bull 52:2,829–2,836. https://doi.org/10.1007/s11434-007-0419-2

Wang YJ, Cheng H, Edwards LR et al (2005) The Holocene Asian monsoon: links to solar changes and North Atlantic climate. Science 308:854–857. https://doi.org/10.1126/science.1106296

Weltje GJ, Prins MA (2003) Muddled or mixed? Inferring palaeoclimate from size distributions of deep-sea clastics. Sediment Geol 162:39–62. https://doi.org/10.1016/S0037-0738(03)00235-5

Wen ZM, Ye W, Ma CM, Zhang YX, Hu ZX (2018) Middle-Late Holocene vegetation history and climate change implied by pollen from Wangdongyang, southern Zhejiang Province, east China. Acta Micropalaeontol Sin 35:260–272 (**in Chinese with English abstracts**)

Wu JY, Wang YJ, Dong JB (2011) Changes in East Asian summer monsoon during the Holocene recorded by stalagmite $\delta^{18}O$ records from Liaoning Province. Quat Sci 31:990–998. https://doi.org/10.3969/j.issn.1001-7410.2011.06.06 (**in Chinese with English abstracts**)

Wu WX, Zheng HB, Hou M, Ge QS (2018) The 5.5 cal ka BP climate event, population growth, circumscription and the emergence of the earliest complex societies in China. Sci China D 61:134–148. https://doi.org/10.1007/s11430-017-9157-1

Xiao JL, Xu QH, Nakamura T, Yang XL, Liang WD, Inouchi Y (2004) Holocene vegetation variation in the Daihai Lake region of north-central China: a direct indication of the Asian monsoon climatic history. Quat Sci Rev 23:1,669–1,679. https://doi.org/10.1016/j.quascirev.2004.01.005

Xie SP, Hu KM, Hafner J, Tokinaga H, Du Y, Huang G, Sampe T (2009) Indian Ocean capacitor effect on Indo-Western Pacific climate during the summer following El Niño. J Clim 22:730–747. https://doi.org/10.1175/2008JCLI2544.1

Xu QH, Zhang SR (2013) Advance in pollen source area. Adv Earth Sci 28:968–975 (**in Chinese with English abstract**)

Yu SY, Berglund BE, Sandgren P, Lambeck K (2007) Evidence for a rapid sea-level rise 7600 yr ago. Geology 35:891–894. https://doi.org/10.1130/G23859A.1

Yue YF, Zheng Z, Huang KY et al (2012) A continuous record of vegetation and climate change over the past 50,000 years in the

Fujian Province of eastern subtropical China. Palaeogeogr Palaeoclimatol Palaeoecol 365–366:115–123. https://doi.org/10.1016/j.palaeo.2012.09.018

Zhao L, Ma CM, Tang LY et al (2016) Investigation of peat sediments from Daiyun Mountain in southeast China: Late Holocene vegetation, climate and human impact. Veget Hist Archaeobot 25:359–373. https://doi.org/10.1007/s00334-016-0554-2

Zhao L, Ma CM, Leipe C et al (2017) Holocene vegetation dynamics in response to climate change and human activities derived from pollen and charcoal records from southeastern China. Palaeogeogr Palaeoclimatol Palaeoecol 485:644–660. https://doi.org/10.1016/j.palaeo.2017.06.035

Zhao L, Ma CM, Xu QM et al (2021) Vegetation evolution in response to climate change and rapid sea-level rise during 8.2–7.0 cal ka bp: pollen evidence from the northwest coast of Bohai Bay, north China. CATENA 196:104,869. https://doi.org/10.1016/j.catena.2020.104869

Zhu C, Ma CM, Yu SY et al (2010) A detailed pollen record of vegetation and climate changes in Central China during the past 16,000 years. Boreas 39:69–76. https://doi.org/10.1111/j.1502-3885.2009.00098.x

Zielhofer C, von Suchodoletz H, Fletcher WJ et al (2017) Millennial-scale fluctuations in Saharan dust supply across the decline of the African Humid Period. Quat Sci Rev 171:119–135. https://doi.org/10.1016/j.quascirev.2017.07.010

Zong Y, Chen Z, Innes JB, Chen C, Wang Z, Wang H (2007) Fire and flood management of coastal swamp enabled first rice paddy cultivation in east China. Nature 449:459–462. https://doi.org/10.1038/nature06135